





Cite this: *J. Anal. At. Spectrom.*, 2024, **39**, 1540

# Comparison and influence of $10^{11}$ and $10^{13}$ ohm resistors used for MC-ICP-MS determination of isotope ratios in highly enriched silicon†

Axel Pramann \* and Olaf Rienitz 

The molar mass  $M$  and isotopic composition of a silicon material highly enriched in  $^{28}\text{Si}$  were measured for the first time using high ohmic ( $10^{13} \Omega$ ) resistors in the feedback loop of amplifiers connected to the Faraday detectors of a multicollector-inductively coupled plasma mass spectrometer (MC-ICP-MS). In the context of the realization and dissemination of the SI units kilogram and mole via the X-ray crystal density (XRCD) method, it is of high importance to maintain and improve the state-of-the-art technique to determine  $M$  with the lowest possible associated uncertainty. The applications and influences of  $10^{11} \Omega$  and  $10^{13} \Omega$  resistors for ion detection were compared using the crystal Si28-33Pr11 exhibiting a large range ( $\approx 10^2$ ) of the ratio  $^{30}\text{Si}/^{29}\text{Si}$ . The low abundance of  $^{30}\text{Si}$  hampers the measurement and thus enlarges the uncertainty. The use of  $10^{13} \Omega$  resistors enables a fourfold dilution of the initial Si sample stock solutions from  $w_{\text{x}}(\text{Si}) = 4536 \mu\text{g g}^{-1}$  down to  $1134 \mu\text{g g}^{-1}$  preserving the MS equipment (ion lenses, slits etc.). A lower limit of  $w_{\text{x}}(\text{Si}) \approx 1134 \mu\text{g g}^{-1}$  for ion currents  $I = 3.4 \text{ fA}$  (corresponding to  $U = 0.34 \text{ mV}$ : gain corrected for  $R = 10^{13} \Omega$ ) for  $^{30}\text{Si}^+$  was determined still maintaining the ability to yield  $u_{\text{rel}}(M) = 4 \times 10^{-9}$ . This will also enable the use of smaller sample sizes, which will considerably reduce costs and time and thus improve this method strongly. Tau correction for  $10^{13} \Omega$  resistors was studied showing no significant influence in case of the continuous beam experiments.

Received 22nd February 2024  
Accepted 1st May 2024

DOI: 10.1039/d4ja00066h  
rsc.li/jaas

## 1 Introduction

The measurement of small ion beams ( $\leq 5 \text{ mV}$  using  $10^{11} \Omega$  resistors) for the determination of isotope ratios in combination with multicollector mass spectrometers (thermal ionisation mass spectrometers (TIMS) and inductively coupled plasma mass spectrometers (ICP-MS)) entered a new era with the introduction and successful application of high ohmic resistors in the feedback loop of Faraday cups used in static measurements.<sup>1–4</sup> The amplifiers equipped with high ohmic resistors – usually with  $R = 10^{13} \Omega$  – enable measurements of extremely small ion beams ( $\leq 5 \text{ mV}$  corresponding to  $3 \times 10^5$  counts per second ( $\text{s}^{-1}$ )), often detected via secondary electron multipliers (SEM). A number of benefits of using  $10^{13} \Omega$  resistors (instead of common  $10^{11} \Omega$  resistors) exist: it is not necessary to use Faraday cups and SEMs in combination, avoiding the inherent problem of cross-calibration of both detector types and thus an increase in measurement uncertainty and experimental efforts. Basically, using a  $10^{13} \Omega$  resistor in contrast to a  $10^{11} \Omega$  resistor leads to a hundredfold gain while the signal to noise ratio merely decreases by a factor of ten, directly influencing the

precision of the measurement, depending on the ion counting statistics and the Johnson–Nyquist noise.<sup>1</sup>

In the case of the  $10^{13} \Omega$  resistors of amplifiers used with Faraday cups, dead-time correction and dark noise determination as in the case of an SEM are not necessary, especially when non-transient signals are measured. If respective small amounts of analytes (low concentration or mass fraction) should be detected, they are now accessible and can be measured, or on the other hand, it is possible to dilute samples further, providing a longer use of stock solutions and/or diluted aliquots. Also, some diluted aggressive matrices are less destructive toward the MS, e.g. the cones and electrostatic lens assemblies are preserved as in the current study.

Several applications of high ohmic resistors using TIMS or MC-ICP-MS have been published in the recent past.<sup>5–12</sup> In the latest generation of the applied MC-ICP-MS (Neptune XT™, Thermo Fisher Scientific GmbH, Bremen, Germany), the gain calibration of the  $10^{13} \Omega$  amplifiers can be performed based on an implemented routine in the operating software. The first application of liquid sample measurements using the  $10^{13} \Omega$  technology within an MC-ICP-MS was reported by Pfeifer *et al.*, who described the determination of Ta isotope ratios yielding an improved uncertainty, previously limited by the low abundance of  $^{180}\text{Ta}$ .<sup>13</sup> A recent example for the applicability of the  $10^{13} \Omega$  technology in case of very limited and low concentration

Physikalisch-Technische Bundesanstalt (PTB), Bundesallee 100, 38116, Braunschweig, Germany. E-mail: axel.pramann@ptb.de

† Electronic supplementary information (ESI) available. See DOI: <https://doi.org/10.1039/d4ja00066h>



sample amounts in bio-medical cerebrospinal fluid was demonstrated by Vanhaecke and coworkers.<sup>14</sup>

In this work, we report the determination of the molar mass and isotopic composition of silicon highly enriched in  $^{28}\text{Si}$  using  $10^{11} \Omega$  and  $10^{13} \Omega$  amplifiers for the first time. Both performances and results were compared with respect to the associated uncertainties. The silicon sample material (crystal Si28-33Pr11) was characterized previously using a standard MC-ICP-MS routine.<sup>15</sup> Silicon highly enriched in  $^{28}\text{Si}$  ( $x(^{28}\text{Si}) > 0.9999 \text{ mol mol}^{-1}$ ) was used as the material of choice for the silicon spheres applied in the context of the X-ray crystal density (XRCD) method which is the underlying primary method for the realization and dissemination of the SI base units the mole and the kilogram.<sup>15–18</sup> A key parameter for the characterization of the respective silicon spheres is the molar mass  $M$  of this very material, which was determined with a relative associated uncertainty  $u_{\text{rel}}(M) < 5 \times 10^{-9}$ . This small uncertainty is only accessible if  $M$  is determined *via* the so-called Virtual-Element Isotope Dilution Mass Spectrometry (VE-IDMS) method, described in detail elsewhere.<sup>19–21</sup> Briefly, only the isotope ratios (in a first step: intensity ratios)  $^{30}\text{Si}/^{29}\text{Si}$  are determined using an MC-ICP-MS. This successful approach has been validated and reported by several national metrology institutes (NMIs) in the past.<sup>22–25</sup>

Since the silicon crystals are extremely enriched in  $^{28}\text{Si}$ , it is an experimental challenge to determine the isotope ratios  $^{30}\text{Si}/^{29}\text{Si}$ . The silicon isotope ratios are  $\approx 10^5$  ( $^{28}\text{Si}/^{29}\text{Si}$ ) and  $\approx 10^7$  ( $^{28}\text{Si}/^{30}\text{Si}$ ) in this study. To symbolise this problem, Fig. 1 shows the (simulated) signal intensities (in V) of the respective Si isotopes as a function of the silicon mass fraction.

Moreover, the extremely small signal intensities of  $^{29}\text{Si}$  and especially  $^{30}\text{Si}$  are accompanied by a ratio of  $x(^{29}\text{Si})/x(^{30}\text{Si}) \approx 100 \text{ mol mol}^{-1}$  in this crystal. The measurement of this ratio using a conventional  $10^{11} \Omega$  amplifier thus requires extremely

high mass fractions of sample  $x$  and blend  $bx$  solutions of  $w_x(\text{Si}) \geq 4000 \mu\text{g g}^{-1}$  and  $w_{bx}(\text{Si}) \geq 1500 \mu\text{g g}^{-1}$  to be able to achieve a reasonable  $^{30}\text{Si}$  signal intensity. It is evident that these mass fractions are usually too high for MC-ICP-MS operations (clogging, surface deposition, contamination...). In this study we concentrated on several aspects: first, comparison of the molar mass and isotopic composition and their associated uncertainties as a function of the resistor connected to the amplifier. Does the use of high-ohmic ( $10^{13} \Omega$ ) resistors influence/improve the uncertainty or at least experimental issues like noise and scattering? Second, the use of highly sensitive  $10^{13} \Omega$  amplifiers for the  $^{29}\text{Si}$  and  $^{30}\text{Si}$  isotope detection opens up the possibility of using more diluted sample aliquots. We prepared Si sample and blend solutions by diluting the initial stock solutions of  $w_x \approx 4500 \mu\text{g g}^{-1}$  and  $w_{bx} \approx 1600 \mu\text{g g}^{-1}$  in order to investigate the quality of the respective isotope ratios. A reasonable lower limit was determined for  $w_x \approx 1100 \mu\text{g g}^{-1}$ . Also, the influence of the blank was investigated. Measurement uncertainties were determined according to the rules of the “Guide to the Expression of Uncertainty in Measurement” (GUM).<sup>26</sup>

## 2. Experimental

### 2.1 Primary method for molar mass determination

Molar mass determinations were performed by the application of the VE-IDMS principle, described in detail elsewhere.<sup>19,21</sup> For a better understanding, only a brief description is given. In order to yield an uncertainty associated with  $M$  which is smaller than  $10^{-8}$ , relatively, only silicon material extremely enriched in  $^{28}\text{Si}$  (almost 100%,  $x(^{28}\text{Si}) > 0.9999 \text{ mol mol}^{-1}$ ) is an option. In this context, also the amount-of-substance fractions  $x$  of the “impurities”  $^{29}\text{Si}$  and  $^{30}\text{Si}$  which are present in very minor traces were determined. Due to the production of this silicon crystal material using gas centrifuges for the enrichment of  $^{28}\text{Si}$  in the initial  $\text{SiF}_4$  gas, not only the absolute fraction of  $x(^{29}\text{Si})$  and  $x(^{30}\text{Si})$  is different from crystal to crystal. Also important to know is the fact that the ratio of  $^{29}\text{Si}$  and  $^{30}\text{Si}$  may vary over several orders of magnitude in different crystals. In this study the crystal Si28-33Pr11 was reexamined.<sup>15</sup> The larger this ratio, the more difficult is its measurement and the larger the uncertainty associated with the isotope ratio  $R$  and the molar mass  $M$ . Thus, using the conventional  $10^{11} \Omega$  technique, very high Si sample concentrations (mass fractions  $w_x > 4000 \mu\text{g g}^{-1}$ ) have been necessary in the past. A possible technical solution for this problem is the application of high ohmic resistors ( $10^{13} \Omega$ ) as presented in this study. Using the VE-IDMS principle, the measurement of the intensity ratios  $^{29}\text{Si}/^{28}\text{Si}$  and  $^{30}\text{Si}/^{28}\text{Si}$  is avoided, because they are several orders of magnitude away from unity. Practically, the VE-IDMS therefore treats the two isotopes  $^{29}\text{Si}$  and  $^{30}\text{Si}$  as a “virtual element” (VE) in the matrix of an extreme excess of  $^{28}\text{Si}$ . Only the isotope ratios  $^{30}\text{Si}/^{29}\text{Si}$  (with the index 2) were determined: in the sample ( $x$ ) of the highly enriched silicon material as well as in the respective blend ( $bx$ ). The latter was prepared from the sample  $x$  and a spike material  $y$  (Si highly enriched in  $^{30}\text{Si}$ ). The respective measured intensity ratios ( $r_{x,2}$  and  $r_{bx,2}$ ) yield sufficiently small uncertainties. Atomic masses of the Si isotopes were taken from the

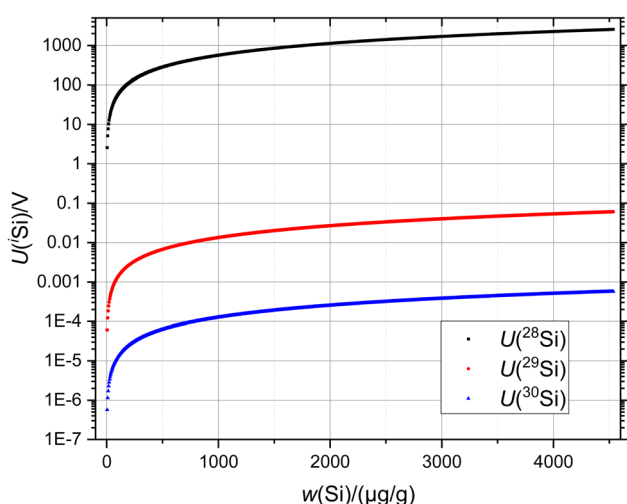


Fig. 1 Simulated intensities (in V, using  $10^{11} \Omega$  amplifiers) of the three stable Si isotopes as a function of the mass fraction  $w$  of Si in the measurement solution. Prior to this study the typical mass fraction of Si was in the range of  $4500 \mu\text{g g}^{-1}$  corresponding to  $U(^{29}\text{Si}) \approx 50 \text{ mV}$  and  $U(^{30}\text{Si}) \approx 0.5 \text{ mV}$  in case of the crystal Si28-33Pr11.



literature.<sup>27</sup> To overcome the inherent problem of mass bias (mass fractionation) when determining isotope ratios, the measured intensity ratios were corrected using calibration factors  $K$ . These were determined experimentally based on binary gravimetric mixtures of silicon parent materials having each a high enrichment in the respective isotope.<sup>20</sup> It was necessary to determine only  $K$  factors used to correct the  $^{30}\text{Si}/^{29}\text{Si}$  ratios ( $K_2$ ). This was done by the measurement of the respective isotope ratio  $r_{w,2}$  of natural silicon ( $w$ ) which was properly characterized with a known “true” isotope ratio  $R_{w,2}$ .<sup>21</sup>

## 2.2 Materials and reagents

The samples used in this study were taken from the silicon crystal material Si28-33Pr11, reported in a previous paper.<sup>15</sup> Thus, the measurements with the  $10^{11} \Omega$  resistors were used for validation purposes complemented by the new results using the  $10^{13} \Omega$  resistors. The general procedure for sample preparation and experimental routines is briefly outlined.

The solid single crystal samples ( $m \approx 500$  mg each) were cleaned and etched prior to digestion with the purpose to remove any contaminations.<sup>21</sup> All bottles and vials (made of PFA: perfluoroalkoxy alkane) were treated by applying a special protocol.<sup>21</sup> Digestion of the etched and weighed samples was performed by dissolution in aqueous tetramethylammonium hydroxide (TMAH) at  $60^\circ\text{C}$  in an ultrasonic bath using TMAH ( $w = 0.25 \text{ g g}^{-1}$ , Alfa Aesar, Thermo Fisher GmbH, Kandel, Germany) of electronic grade purity (99.9999%). The stock

solutions were prepared by dilution using purified water ( $18 \text{ M}\Omega \text{ cm}$  resistivity; water purification system: Merck Millipore™). The mass fractions of the solvent TMAH of all solutions (samples, blank) were  $w(\text{TMAH}) = 0.0006 \text{ g g}^{-1}$ . The range of the isotopic abundance between  $^{28}\text{Si}$  and  $^{30}\text{Si}$  is extremely large and covers 7 orders of magnitude in this crystal; therefore, for the usual measurement (with  $10^{11} \Omega$  resistors, and as in previous measurements) it was necessary to start with very high mass fractions  $w_{x,0}(\text{Si}) = 4536 \mu\text{g g}^{-1}$  and  $w_{bx,0}(\text{Si}) = 1507 \mu\text{g g}^{-1}$  (in case of subsample V.2.3). The blend bx denotes the blend consisting of the sample x and spike material y. For the  $K$  factor determination material w with  $w_w(\text{Si}) = 4 \mu\text{g g}^{-1}$  was used. In order to investigate the possibility of diluting the initial stock solution and blend, the starting mass fractions were diluted  $w_x/(\mu\text{g g}^{-1})$ :  $4536 \rightarrow 2268 \rightarrow 1134 \rightarrow 567 \rightarrow 284$ ;  $w_{bx}/(\mu\text{g g}^{-1})$ :  $1507 \rightarrow 754 \rightarrow 377 \rightarrow 188 \rightarrow 94$ . Due to the contamination with omnipresent Si of natural isotopic composition and to correct for carry-over effects, the blank signals (measured prior to the sample or blend) were subtracted from the respective signals.

## 2.3 Mass spectrometry and data evaluation

The isotope ratio measurements of the enriched silicon samples were performed with a high resolution multicollector-inductively coupled plasma mass spectrometer (MC-ICP-MS) Neptune™ XT (Thermo Fisher Scientific GmbH, Bremen, Germany).<sup>13,15</sup> Generally, the samples were measured as similar as in a previous study, where  $10^{11} \Omega$  resistors connected to

**Table 1** Operation conditions of the Neptune XT™ MC-ICP-MS

Vacuum generation	Scroll pump, turbo pumps, jet pump (almost oil-free)
Sample introduction	50 $\mu\text{L min}^{-1}$ PFA nebulizer Cyclonic and Scott chamber (PEEK/PFA) Sapphire torch and injector, sapphire bonnet, Ni X-skimmer and Ni sampler
Gas flow rates (argon 5.0)	Cooling: 16 $\text{L min}^{-1}$ , auxiliary: 0.8 $\text{L min}^{-1}$ , sample: 1.0 $\text{L min}^{-1}$
Machine settings	Pseudo high resolution HR ( $M/\Delta M = 8000$ ) Plasma power $P(\text{RF}) = 1180 \text{ W}$
Autosampler	CETAC ASX 110 FR
Sequence settings	Rinse time: 120 s Take-up time: 60 s, measured samples/sequence: x, bx, w (4 times each)
Blank measurement	Prior to each sample

**Table 2** Parameters used with the different resistor setups

	$10^{11} \Omega$ amplifier	$10^{13} \Omega$ amplifier
$w_x$ range (approx.)/( $\mu\text{g g}^{-1}$ )	4500–4700	4500–4700, 2300, 1100, 550, 280
Faraday detectors	C: $^{29}\text{Si}^+$ , H3: $^{30}\text{Si}^+$ $^{28}\text{Si}^+$ : detectors moved out of the beam	C: $^{29}\text{Si}^+$ , H3: $^{30}\text{Si}^+$ $^{28}\text{Si}^+$ : detectors moved out of the beam
Amplifier no.	C: 2, H3: 8	C: 9, H3: 10
Gain	Both: $10^0$	Both: $10^{-2}$
Tau constant/s	Ampl. 2: 0.11; ampl. 8: 0.10	Ampl. 9: 0.61; ampl. 10: 0.53
Operation mode	Static	Static
Rotating amplifiers	Applied/not applied	Not applied
Integration time/s	4.194	8.389
Idle time/s	3.000	10.00
Number of integrations	1	1
Number of cycles/block	3	3
Number of blocks	6	6



amplifiers (in a rotating mode) were used.<sup>15</sup> In Table 1, the typical operation conditions and in Table 2 the respective amplifier settings are shown. Since isotope ratios of silicon artificially highly enriched in <sup>28</sup>Si and simultaneously depleted in <sup>29</sup>Si and <sup>30</sup>Si were determined, a sample introduction system manufactured from PFA/PEEK and an ICP torch with sapphire parts and a sapphire injector were used. Additionally, contaminations of the procedural blank introduced by the solvent were corrected for by subtracting the blank signals measured prior to the sample from the latter. This, however, might cause some trouble by blank overcorrection when the concentration of the analyte in the sample decreases. In case of the 10<sup>11</sup> Ω amplifier configuration (see Table 2), the total measurement duration (one sequence) was approximately 2.5 hours (blank – sample (four times); blank – blend (four times); blank – nat.-Si (four times)). Generally, a short sequence is preferable when measuring enriched silicon in high resolution to avoid potential mass-drift effects.<sup>28</sup>

The total measurement time increases to 3.5 hours when using the 10<sup>13</sup> Ω amplifiers. In the latter case, the high ohmic resistors cause a slower response time of the amplifiers (so that a longer integration time (8.4 s) and idle time (10 s) are necessary).<sup>13</sup> In case of the 10<sup>13</sup> Ω amplifier configuration, the software-based gain calibration takes three hours.

### 3. Results and discussion

#### 3.1 Statistical comparison of 10<sup>11</sup> Ω and 10<sup>13</sup> Ω amplifiers: isotope ratio measurements

The isotope ratios  $R_x = x(^{30}\text{Si})/x(^{29}\text{Si})$  in the sample N.2.1 ( $w = 4710 \mu\text{g g}^{-1}$ ) and  $R_{\text{bx}} = x(^{30}\text{Si})/x(^{29}\text{Si})$  in the blend bx are shown for the individual sequences and the respective amplifier settings (10<sup>11</sup> Ω, with amplifier rotation; 10<sup>11</sup> Ω, no amplifier rotation; 10<sup>13</sup> Ω, no amplifier rotation) in Fig. 2. The respective raw data and calculations are given in the ESI † where the calculations can be retraced. In case of  $R_x$ , the data are consistent for  $k = 2$  showing a larger scattering especially in case of the 10<sup>11</sup> Ω setup with rotating amplifiers. Error bars denote the standard uncertainties ( $k = 1$ ) without scattering contributions. For comparison of the  $R = 10^{11}$  Ω and the  $R = 10^{13}$  Ω setups at a first glance, the two setups without rotating amplifiers are more suitable. Contrary to expectations, the relative combined uncertainties associated with  $R_x$  and  $R_{\text{bx}}$  are twice as large in case of the  $R = 10^{13}$  Ω setups than in case of the  $R = 10^{11}$  Ω setups. Generally,  $u_{\text{c,rel}}$  is smaller in case of  $R_{\text{bx}}$  compared to  $R_x$  by a factor of at least 50 due to the numerical value of  $R_{\text{bx}}$  which is much closer to unity.

In the high concentration range of the sample ( $w_x = 4000$ – $5000 \mu\text{g g}^{-1}$ ), the application of 10<sup>13</sup> Ω resistors will not improve the uncertainties in  $R$ .

However, in case of the enriched Si material, the main intention is the determination of the molar mass  $M$  and its associated uncertainty. Therefore, the impact of the different resistors on this quantity is of main interest and will be discussed in the following.

Fig. 3 shows the molar mass distribution of measurements of the subsample N.2.1 ( $w = 4710 \mu\text{g g}^{-1}$ ). The measurements

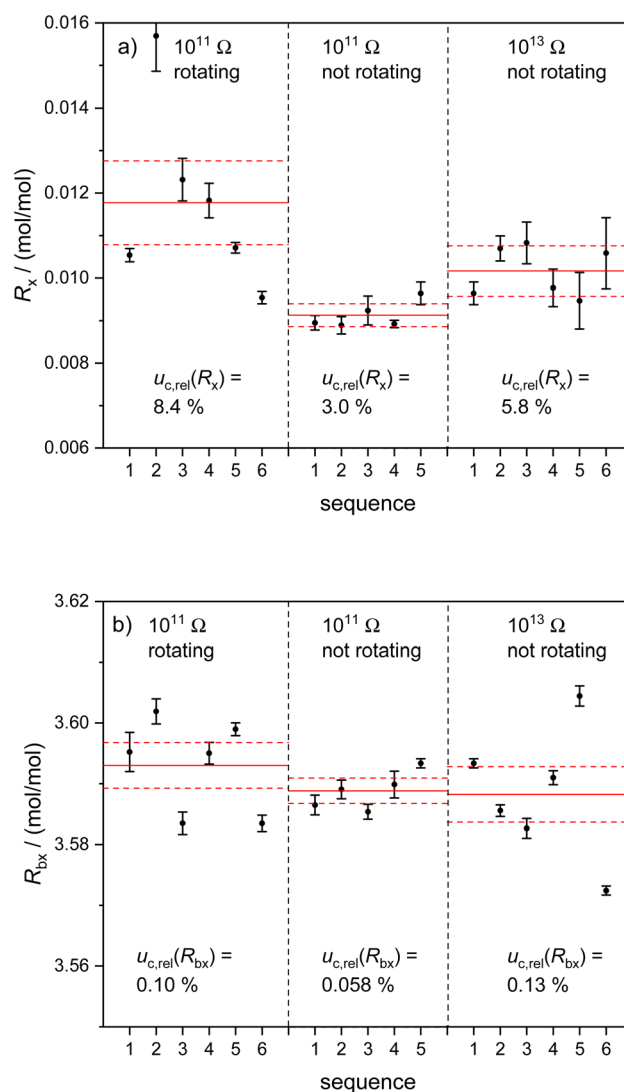


Fig. 2 Isotope ratios  $R_x$  (a) in the sample N.2.1 ( $w = 4710 \mu\text{g g}^{-1}$ ) and  $R_{\text{bx}}$  (b) in the blend for the individual sequences using three different amplifier settings. Cups C and H3: 10<sup>11</sup> Ω resistors (with and without rotating amplifiers), 10<sup>13</sup> Ω resistors (without rotating amplifiers). Error bars denote associated standard uncertainties ( $k = 1$ ). Red solid lines: average  $R_x$ ,  $R_{\text{bx}}$ . Red dashed lines: upper and lower average of  $u(R)$  with  $k = 1$  including data scattering contribution.

were performed in the same way as reported previously using the 10<sup>11</sup> Ω amplifier setting with rotating virtual amplifiers.<sup>15</sup> Using the 10<sup>11</sup> Ω resistors and rotating virtual amplifiers (Fig. 3 left), an average value  $M = 27.976949950(54) \text{ g mol}^{-1}$  was obtained with  $u_{\text{rel}} = 1.9 \times 10^{-9}$  (the last digits denote the combined uncertainty  $u_c$  associated with  $M$ ,  $k = 1$ ).

This value is  $4.2 \times 10^{-7} \text{ g mol}^{-1}$  below the value reported previously due to a long-term TMAH-leaching and new type sapphire-torch removing natural silicon even more efficiently.<sup>15</sup> The respective measurement results without rotating amplifiers (Fig. 3 centre) yield  $M = 27.976\,949\,839(50) \text{ g mol}^{-1}$  with  $u_{\text{rel}} = 1.8 \times 10^{-9}$ .

This series was measured as a proof of data consistency when applying/not applying the virtual amplifier concept





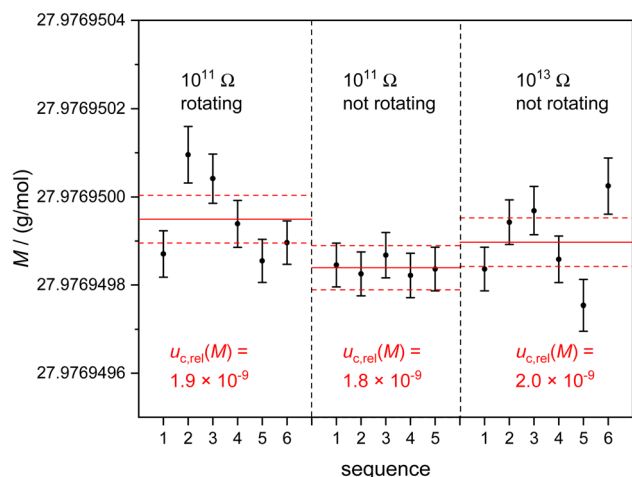


Fig. 3 (Left) Molar masses measured in sample N.2.1 ( $w = 4710 \mu\text{g g}^{-1}$ ) with  $10^{11} \Omega$  resistors (cups C and H3) with virtual amplifier rotation. Error bars denote associated uncertainties ( $k = 1$ ). Red solid line: average molar mass. Red dashed lines: upper and lower average of  $u(M)$  with  $k = 1$ . (Centre) Same as left using  $10^{11} \Omega$  resistors (cups C and H3) without virtual amplifier rotation. (Right) Same as centre using  $10^{13} \Omega$  resistors (cups C and H3).

developed by Thermo Fisher Scientific™, which was introduced for the reduction of biases due to the gain calibration.

No significant difference in the data sets was observed within the limits of uncertainty, because main uncertainty

contributions result from intensity ratios obtained from extremely different isotope abundances of the enriched material as will be outlined later. In the right part of Fig. 3 the respective molar mass results are shown using the  $10^{13} \Omega$  resistors connected to cups C and H3. Here,  $M = 27.976\,949\,898(55) \text{ g mol}^{-1}$  with  $u_{\text{rel}} = 2.0 \times 10^{-9}$  was obtained. All three measurements ( $10^{11} \Omega$  and  $10^{13} \Omega$  resistors, virtual amplifier concept applied and not applied) agree within the limits of uncertainty. The underlying raw data and calculations are given in the respective Excel™ sheets of the ESI 1.†

Regarding the uncertainty of the molar mass of enriched silicon, no significant change was observed when using the high ohmic resistor setting. Table 3 shows representative uncertainty budgets of sample N.2.1 of a single sequence using:  $10^{11} \Omega$  resistors with and without rotating amplifiers as well as  $10^{13} \Omega$  resistors without rotating amplifiers. The uncertainty budgets were calculated using the GUM Workbench Pro™ software (version 2.4.1 392; Metrodata GmbH, Germany) according to guidelines of the GUM.<sup>26</sup>

The budgets are rather similar and differences can only be observed in small variations in the measured intensity ratios  $r_{x,2}$  (sample),  $r_{\text{bx},2}$  (blend of sample x and “Si30” spike y), and  $r_{w,2}$  (natural Si w for  $K$  factor determination). From those, no clear indication can be derived if the high ohmic amplifiers will have a more positive impact on  $u(M)$ .

An explanation will be the fact that the molar mass  $M$  is a result of the complex “Virtual-Element IDMS” principle, which is only in a minor part dependent on the intensity ratios

Table 3 Representative uncertainty budgets of  $M$  with different resistors. I:  $10^{11} \Omega$ , rotating amplifiers; II:  $10^{11} \Omega$ , not applying rotating amplifiers; III:  $10^{13} \Omega$ , not applying rotating amplifiers. Respective atomic masses were taken from ref. 27

Amplifier setting	Quantity	Unit	Best estimate (value)	Standard uncertainty	Sensitivity coefficient	Index (%)
	$X_i$	$[X_i]$	$x_i$	$u(x_i)$	$c_i$	
I, II, III	$M(^{28}\text{Si})$	$\text{g mol}^{-1}$	27.976926534940	$540 \times 10^{-12}$	1.0	0.0
	$m_{\text{yx}}$	g	$5.611000 \times 10^{-6}$	$704 \times 10^{-12}$	4.2	0.3
	$m_x$	g	0.062474995	$569 \times 10^{-9}$	$-370 \times 10^{-6}$	0.0
	$M(^{29}\text{Si})$	$\text{g mol}^{-1}$	28.976494669090	$610 \times 10^{-12}$	$23 \times 10^{-6}$	0.0
	$R_{y,3}$	$\text{mol mol}^{-1}$	1.5855	0.0222	$-80 \times 10^{-9}$	0.1
	$M(^{30}\text{Si})$	$\text{g mol}^{-1}$	29.9737701360	$27.0 \times 10^{-9}$	$-500 \times 10^{-9}$	0.0
I					$-560 \times 10^{-9}$	0.0
II					$-550 \times 10^{-9}$	0.0
III					$-550 \times 10^{-9}$	0.0
I	$R_{y,2}$	$\text{mol mol}^{-1}$	269.04	5.65	$2.0 \times 10^{-9}$	4.3
II						4.6
III						4.4
I	$R_{w,2}$	$\text{mol mol}^{-1}$	0.66230	$1.32 \times 10^{-3}$	$-35 \times 10^{-6}$	75.7
II						81.5
III						76.8
I	$r_{x,2}$	V/V	0.012470	$405 \times 10^{-6}$	$50 \times 10^{-6}$	14.2
II			0.009800	$342 \times 10^{-6}$	$49 \times 10^{-6}$	10.7
III			0.010400	$439 \times 10^{-6}$	$49 \times 10^{-6}$	16.5
I	$r_{\text{bx},2}$	V/V	3.79034	$1.90 \times 10^{-3}$	$-6.3 \times 10^{-6}$	5.00
II			3.80227	$1.14 \times 10^{-3}$	$-6.2 \times 10^{-6}$	1.9
III			3.82259	$1.15 \times 10^{-3}$	$-6.2 \times 10^{-6}$	1.8
I	$r_{w,2}$	V/V	0.6982900	$90.8 \times 10^{-6}$	$33 \times 10^{-6}$	0.3
II			0.702370	$140 \times 10^{-6}$	$33 \times 10^{-6}$	0.8
III			0.7050200	$56.4 \times 10^{-6}$	$33 \times 10^{-6}$	0.1
I	$M$	$\text{g mol}^{-1}$	27.9769499399	$53.3 \times 10^{-9}$		
II			27.9769498685	$51.5 \times 10^{-9}$		
III			27.9769498590	$52.9 \times 10^{-9}$		



(isotope ratios) directly, which are influenced by the kind of resistor chosen.

The influence of the  $10^{11} \Omega$  and  $10^{13} \Omega$  resistors in the case of highly enriched silicon solutions was analysed statistically by comparing the measured intensity ratios  $r = U(^{30}\text{Si})/U(^{29}\text{Si})$  in the sample solutions x, the blend solution bx, and the calibration solution w of sample N.2.1 using the initial sample concentrations ( $w_x = 4710 \mu\text{g g}^{-1}$ ;  $w_{bx} = 1510 \mu\text{g g}^{-1}$ ;  $w_w = 4 \mu\text{g g}^{-1}$ ). For each solution, up to six sequences were measured, each yielding an average intensity ratio with an associated experimental standard deviation of the mean  $s$  according to the GUM.<sup>26</sup> For a better comparison, the not-blank corrected ratios are discussed only. The data sets and evaluation procedures are given in the respective Excel™ sheets of the ESI 2.† Fig. 4a–c show the relative standard deviations of the mean  $s_{\text{rel}}$  of the intensity ratios  $r$  in solutions x, bx, and w, measured with  $10^{11} \Omega$  and  $10^{13} \Omega$  equipped amplifiers.

In case of the sample solution x (highly enriched Si), the relative experimental standard deviations  $r = U(^{30}\text{Si})/U(^{29}\text{Si})$  are almost equal when using the  $10^{11} \Omega$  or  $10^{13} \Omega$  setup with a small benefit of the  $10^{11} \Omega$  resistors. A possible reason might be the intrinsic scattering of the intensity ratios  $r_x (\approx 0.01 \text{ V/V})$  in case of the sample material with an isotope ratio  $R_x \approx 0.009 \text{ mol mol}^{-1}$ , two orders of magnitude away from unity, even if the absolute  $^{30}\text{Si}$  signal is in the lower mV range. An advantage of the  $10^{13} \Omega$  amplifier setup can be observed in the ratios of the blend bx with  $R_{bx} \approx 4 \text{ mol mol}^{-1}$ . Here, the respective course of the relative experimental standard deviations of the mean  $s_{\text{rel}}$  is smoother and with an average of 0.0073% lower than in case of the  $10^{11} \Omega$  setup (0.0095%) due to the absolute ratio near unity. In case of the solution w, the impact of the setup ( $10^{11} \Omega$  or  $10^{13} \Omega$ ) is very similar, due to the much larger signal intensities (silicon with almost natural isotopic distribution) and an intensity ratio  $r_w \approx 0.7 \text{ V/V}$ .

### 3.2 Comparison of $10^{11} \Omega$ and $10^{13} \Omega$ amplifiers: influence of sample mass fraction

However, the application of the high-ohmic resistors should enable accurate and precise measurements of lower concentrated or diluted samples. For this reason, different concentrations of the subsample V.2.3 were measured using original and diluted aliquots of x and bx ( $w_{x,0} = 4536 \mu\text{g g}^{-1}$ ;  $w_{bx,0} = 1507 \mu\text{g g}^{-1}$ ) keeping  $w_w$  constant (compare Section 2.2). Fig. 5 displays the results of the molar mass determinations comparing the original measurement from 2020 (ref. 15) ( $w_x = 4536 \mu\text{g g}^{-1}$  with  $10^{11} \Omega$  amplifiers, 6 sequences) with the recent measurements using the  $10^{13} \Omega$  amplifier setup. The latter were measured using the following mass fractions w:  $4536 \mu\text{g g}^{-1}$  (6 sequences),  $2268 \mu\text{g g}^{-1}$  (6 sequences), and  $1134 \mu\text{g g}^{-1}$  (4 sequences due to the sample running out of stock). The average molar mass of these very samples was determined as the arithmetic mean of the two  $4536 \mu\text{g g}^{-1}$  ( $10^{11} \Omega$  and  $10^{13} \Omega$ ) and the  $1134 \mu\text{g g}^{-1}$  ( $10^{13} \Omega$ ) measurements including the contribution of data scattering. The solid black line denotes the average value  $M(\text{V.2.3}) = 27.97695056(14) \text{ g mol}^{-1}$  (the last two digits represent the uncertainty associated with  $M$ ,  $k = 1$ ). This corresponds

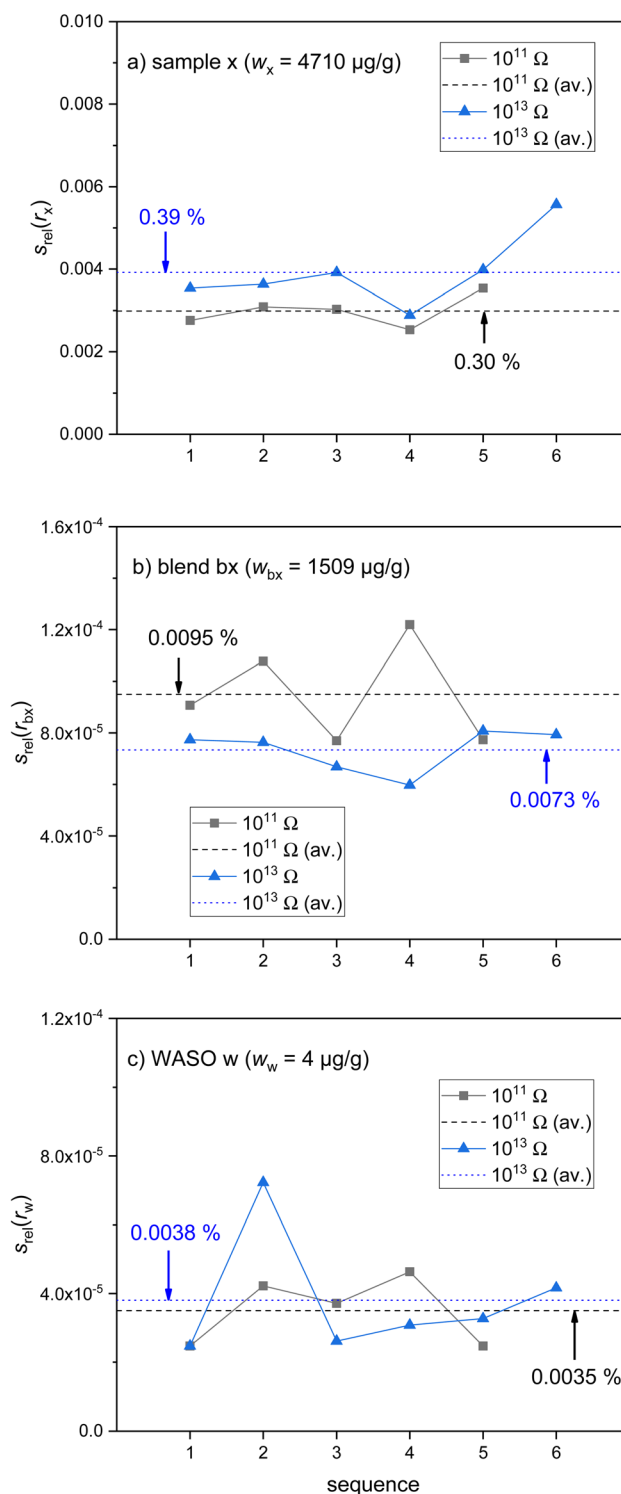


Fig. 4 (a–c) Comparison of  $10^{11} \Omega$  and  $10^{13} \Omega$  amplifier setups applied for the determination of signal intensity ratios  $r = (U(^{30}\text{Si})/U(^{29}\text{Si}))$  in the three solutions x, bx, and w (subsample N.2.1 without dilution). As a measure of the statistical quality, the relative experimental standard deviation of the mean  $s_{\text{rel}}$  of these ratios is plotted vs. the respective sequence. Single data are given in black squares ( $10^{11} \Omega$ ) and blue triangles ( $10^{13} \Omega$ ). Respective averages are shown via black dashed ( $10^{11} \Omega$  average) and blue dotted lines ( $10^{13} \Omega$  average).

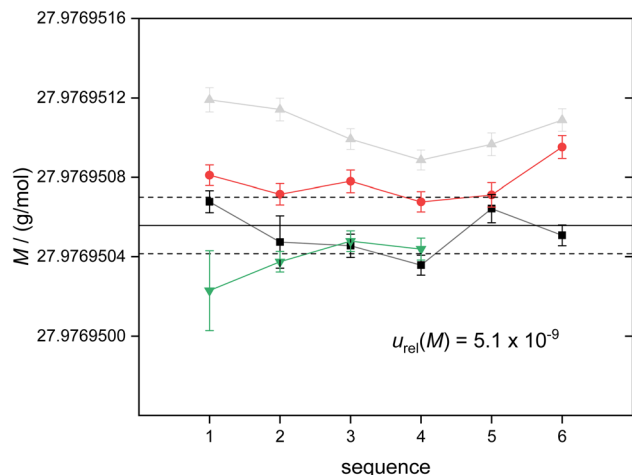


Fig. 5 Comparison of molar mass determinations of the sample Si28-33Pr11V.2.3: 4536  $\mu\text{g g}^{-1}$  (black squares,  $10^{11} \Omega$ , 2020 (ref. 15)); 4536  $\mu\text{g g}^{-1}$  (red circles,  $10^{13} \Omega$ ); 2268  $\mu\text{g g}^{-1}$  (grey triangles,  $10^{13} \Omega$ ); 1134  $\mu\text{g g}^{-1}$  (green triangles,  $10^{13} \Omega$ ). The solid black line denotes the arithmetic mean of the two 4536  $\mu\text{g g}^{-1}$  and the 1134  $\mu\text{g g}^{-1}$  data sets. The dotted lines denote the respective upper and lower uncertainty limits (including data scattering,  $k = 1$ ).

to a relative uncertainty  $u_{\text{rel}}(M) = 5.1 \times 10^{-9}$ . The data set of the 2268  $\mu\text{g g}^{-1}$  measurement ( $10^{13} \Omega$ , greyed out in Fig. 5) was not used for the calculation of  $M$  due to a slight offset resulting from a tentative contamination with natural silicon during dilution. The average value of  $M(\text{V.2.3})$  agrees with the former value reported in ref. 15 within the limits of uncertainty. The data sets as well as their compilation are also available in the ESI 3.†

The consistency of these data sets was analysed using the principle of the degrees-of-equivalence ( $d_i$ ).

$$d_i = M_i - M \quad (1)$$

with the molar mass  $M_i$  of the respective sequence and the arithmetic mean  $M$ . The expanded uncertainties  $U(d_i)$  ( $k = 2$ ) associated with  $d_i$  were determined according to eqn (2):

$$U(d_i) = 2 \times \sqrt{u^2(M_i) + u^2(M)} = 2 \times \sqrt{u^2(M_i) + \frac{\sum_{i=1}^N u^2(M_i)}{N}} \quad (2)$$

Fig. 6 shows the  $d_i$  and associated uncertainties  $U(d_i)$  comparing the four data sets (including the scattering contribution in the respective uncertainty bars).

The data sets can be regarded as consistent if the individual  $d_i$  are smaller than their uncertainties. This criterion is fulfilled for almost all data points except several of the 2268  $\mu\text{g g}^{-1}$  data. For consistency, the error bars should encompass the zero line (red line in Fig. 6). Therefore, the data set of the 2268  $\mu\text{g g}^{-1}$  measurement was not included in the molar mass evaluation for the subsample V.2.3.

The influence of the different resistor settings was analysed by comparing the statistical impact on the relative experimental

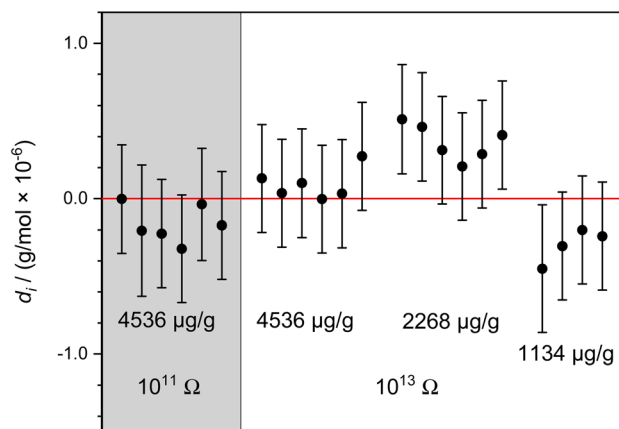


Fig. 6 Degrees of equivalence  $d_i$  of the four data sets of the molar mass measurements of the subsample Si28-33Pr11V.2.3: 4536  $\mu\text{g g}^{-1}$  ( $10^{11} \Omega$ , grey area); 4536  $\mu\text{g g}^{-1}$  ( $10^{13} \Omega$ ); 2268  $\mu\text{g g}^{-1}$  ( $10^{13} \Omega$ ); and 1134  $\mu\text{g g}^{-1}$  ( $10^{13} \Omega$ ). The expanded uncertainties  $U(d_i)$  associated with  $d_i$  are displayed as error bars.

standard deviations of the mean  $s_{\text{rel}}$  of the measured intensity ratios  $r = U(^{30}\text{Si})/U(^{29}\text{Si})$  in the sample  $x$ , the blend  $\text{bx}$ , and the natural Si solution  $w$ . In case of the  $10^{13} \Omega$  amplifier settings, the additional dependence on the dilution of the sample  $x$  (4536, 2268, and 1134  $\mu\text{g g}^{-1}$ ) is shown in Fig. 7.

Generally, the  $s_{\text{rel}}$  for  $r_{\text{bx}}$  and  $r_w$  are in a range below 0.030% which is not significantly dependent on the mass fraction  $w$ . In case of the  $10^{13} \Omega$  resistors, a decrease of  $s_{\text{rel}}(r_w)$  can be observed by a factor of ten ( $<0.0050\%$ ) compared to the  $10^{11} \Omega$  resistors. For  $r_{\text{bx}}$ , the range is almost constant (0.075%–0.015%) independent from the mass fraction. The 2268  $\mu\text{g g}^{-1}$  data set also shows the statistical quality and ability of this mass fraction compared to the original 4536  $\mu\text{g g}^{-1}$  solution.

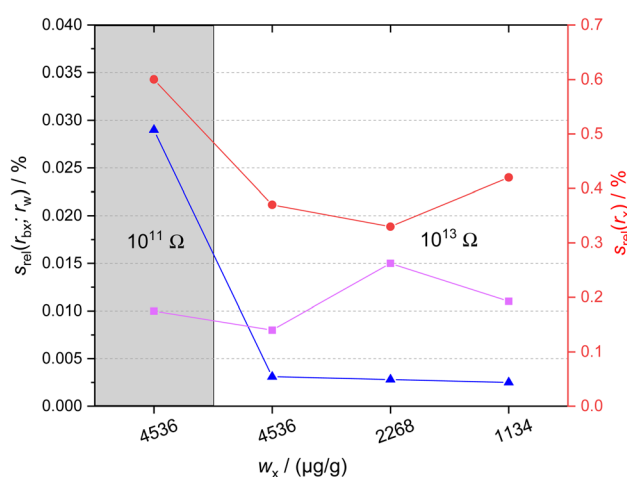


Fig. 7 Comparison of the relative experimental standard deviations of the mean of the intensity ratios  $r$  in the sample  $x$  (subsample V.2.3; red circles, right y-axis), blend  $\text{bx}$  (subsample V.2.3, magenta squares, left y-axis), and natural Si  $w$  (blue triangles, left y-axis). In case of  $10^{13} \Omega$  resistors, results are shown for the different mass fractions of the sample  $w_x = 4536, 2268$ , and  $1134 \mu\text{g g}^{-1}$ . The grey shaded area refers to the  $10^{11} \Omega$  measurements ( $w_x = 4536 \mu\text{g g}^{-1}$ ).



In case of  $r_x$ , the respective  $s_{\text{rel}}$  are in a higher range between 0.30% and 0.45% when using the  $10^{13} \Omega$  resistors, independent of the mass fraction used. Since the measurement of intensity (and isotope) ratios  $r_x$  is affected by larger uncertainties, the use of  $10^{13} \Omega$  instead of  $10^{11} \Omega$  amplifiers will not significantly improve the statistical quality of the data  $s_{\text{rel}}(r_x)$ .

Further dilutions of samples with  $w_x = 567 \mu\text{g g}^{-1}$  and  $w_x = 284 \mu\text{g g}^{-1}$  could not be measured even when using  $10^{13} \Omega$  amplifiers, because the absolute signal intensities of  $^{29}\text{Si}$  and  $^{30}\text{Si}$  in the sample solutions were in the same range as in the blank solution. For this reason,  $w_x = 1134 \mu\text{g g}^{-1}$  can be regarded as an approximate lower limit of the mass fraction for the measurement of  $M$  using the  $10^{13} \Omega$  amplifier set up for this special silicon crystal.

As one main result the application of high ohmic  $10^{13} \Omega$  resistors instead of  $10^{11} \Omega$  resistors is enabling the measurement of at least fourfold diluted samples (from  $4536 \mu\text{g g}^{-1}$  down to  $1134 \mu\text{g g}^{-1}$ ). To give an overview of the absolute intensities (voltages and ion currents), Table 4 lists typical data generated with sample V.2.3 using the  $10^{11} \Omega$  and  $10^{13} \Omega$  setup. The voltages in case of the  $10^{13} \Omega$  resistors were gain factor-corrected to enable a direct comparison with the values obtained with the  $10^{11} \Omega$  resistors.<sup>1</sup> It can be observed that the overall dynamic range of the  $10^{13} \Omega$  resistors covers three orders of magnitude yielding in case of the  $^{30}\text{Si}^+$  ion an ion current of a few fA which is still sufficient for molar mass determinations.

The use of high ohmic resistors is directly correlated with experimental benefits: fast clogging of the sampler and skimmer cones is avoided due to lower analyte concentrations; a more stable signal quality is generated, and the mass spectrometer can be operated in a less aggressive concentration regime. The other main outcome when using the  $10^{13} \Omega$  resistors is the fact, that a strongly reduced sample mass (down to  $m(\text{crystal}) \approx 125 \text{ mg}$  corresponding to  $w \approx 1000 \mu\text{g g}^{-1}$ ) will be sufficient in the future for the measurement of the molar mass and isotopic composition of silicon enriched in  $^{28}\text{Si}$ : a mass of approximately 125 mg solid Si will yield 125 g of a solution with  $w \approx 1000 \mu\text{g g}^{-1}$  (instead of 500 mg Si needed to prepare a solution of 125 g with  $w \approx 4000 \mu\text{g g}^{-1}$ ). This will save time and costs for sample preparation and material consumption. Moreover, a smaller crystal sample (size) might enable a better

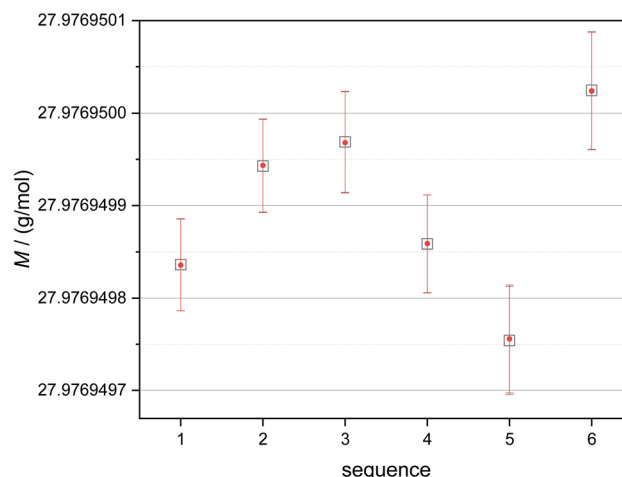


Fig. 8 Molar mass distributions of subsample N.2.1 over six sequences. Open squares: not tau corrected data; red circles: tau corrected data. No significant difference can be observed.

space resolved sample characterization. This will improve the insight into the homogeneity of the isotopic composition of the respective crystals underpinning their ability for the use in the XRCd method.

### 3.3 Investigation of mass bias due to signal delay impact – tau correction

In MC-ICP-MS there are several sources for biased isotope ratios. The analogue currents, generated in the Faraday cups by release of charge create a voltage on the respective (high ohmic) resistor. These voltages are converted to frequencies using a voltage-to-frequency converter. Thus, even in a multicollector detection system very short time-offsets of the different detector outputs are generated due to different signal decays which depend on the “first-order-tau-constant” of the respective resistor.<sup>11,12,29–32</sup> When using high ohmic resistors (e.g.  $10^{13} \Omega$ ), this time delay between the incoming signal and detector response times (detector decay duration) might generate a bias in isotope ratios – especially in case of transient signals. A test of a potential influence of the tau correction using the  $10^{13} \Omega$  resistors was applied. The tau constants (symbol  $\tau$ ) of each amplifier – initially generated during machine installation – were taken from the software-based tau decay constants listed in the Neptune XT™ software (executive tool).<sup>29</sup> For the test measurements, the N.2.1 subsample ( $w = 4710 \mu\text{g g}^{-1}$ ) was used. The C and H3 cups were operated with  $10^{13} \Omega$ ; six sequences were measured each.

For the tau corrected ion signal  $I_{\text{corr}}(t_i)$  at the time  $t_i$ , the following expression was used:

$$I_{\text{corr}}(t_i) = I_m(t_i) + \frac{I_m(t_{i+1}) - I_m(t_{i-1})}{t_{i+1} - t_{i-1}} \times \tau \quad (3)$$

with the measured intensities of the respective isotope  $I_m(t_i)$  at the time  $t_i$ ,  $I_m(t_{i+1})$  at the successive time  $t_{i+1}$ ,  $I_m(t_{i-1})$  of the preceding time  $t_{i-1}$  and the tau constant  $\tau$ .<sup>11,14,29</sup> The following tau constants were used for the respective amplifiers: amplifier 9 (cup C):  $\tau = 0.6061 \text{ s}$ ; amplifier 10 (cup H3):  $\tau = 0.5266 \text{ s}$

Table 4 Comparison of typical absolute signal intensities of sample V.2.3 (in V, ion currents in fA of the  $^{29}\text{Si}^+$  and  $^{30}\text{Si}^+$  signals measured at different mass fractions (dilution steps) using the  $10^{11} \Omega$  and  $10^{13} \Omega$  amplifier setups. In case of the  $10^{13} \Omega$  measurements, the voltage data were gain factor-corrected

$w_x (\mu\text{g g}^{-1})$		$R/\Omega$	$U/V$	$I/\text{fA}$
4536	$^{29}\text{Si}^+$	$10^{11}$	0.13542	1354
	$^{30}\text{Si}^+$	$10^{11}$	0.00140	13.96
4536	$^{29}\text{Si}^+$	$10^{13}$	0.11326	1133
	$^{30}\text{Si}^+$	$10^{13}$	0.00109	11
2268	$^{29}\text{Si}^+$	$10^{13}$	0.04050	405
	$^{30}\text{Si}^+$	$10^{13}$	0.00062	6.2
1134	$^{29}\text{Si}^+$	$10^{13}$	0.02283	228
	$^{30}\text{Si}^+$	$10^{13}$	0.00034	3.4





(compare Table 2). For the calculation of the time intervals, the exported raw data (absolute time in s) of the respective method generated by the "Data Evaluation" application of the NeptuneXT<sup>TM</sup> software were taken, defined by the selected integration time (8.39 s). Thus, the basic time interval is 8.39 s. However, the next two following time intervals are increased (13.8 s or 14.8 s), followed periodically by the initial time interval of 8.39 s and so forth. For the corrected ion signal  $I_{\text{corr}}(t_i)$ , the respective time intervals were used. Data evaluation processes as well as raw data and uncertainties for tau correction can be found in an Excel<sup>TM</sup> sheet of the ESI 4.†

After measuring six sequences of the sample N.2.1 and applying tau correction, an almost identical course of the

corrected molar masses  $M_\tau$  and their associated uncertainties as in the case of not tau corrected measurements ( $M_{n\tau}$ ) was obtained (see Fig. 8).

The absolute differences  $\Delta M$  between  $M_{n\tau}$  and  $M_\tau$  are shown in Fig. 9.

The  $\Delta M$  values are located in the lower  $10^{-9}$  g mol<sup>-1</sup> range (Fig. 9b). For comparison, in Fig. 9a, the area covered with the average uncertainty associated with  $M$  is bracketed by the red dashed lines. The latter covers a range approximately a factor twenty larger than  $\Delta M$ . Therefore, application of tau correction in case of the  $10^{13}$   $\Omega$  resistors does not influence the isotope ratios as well as the respective molar mass in the current study in any way. This is mainly based on the use of stable signal inputs (continuous ion beams) rather than transient signals as apparent when coupling the MS to a laser ablation or any kind of chromatography. Therefore, additional tau correction shows no significant advantages for the current study.

## 4. Conclusions

The current determination of the molar masses of different subsamples of the enriched silicon crystal Si28-33Pr11 with a large ratio  $^{29}\text{Si}/^{30}\text{Si} > 100$  using amplifier setups with  $10^{11}$   $\Omega$  and  $10^{13}$   $\Omega$  for the first time has produced several main outcomes: First, a direct comparison of the same sample with the original high analyte mass fraction of  $w > 4500$   $\mu\text{g g}^{-1}$  using  $10^{11}$   $\Omega$  and  $10^{13}$   $\Omega$  amplifiers shows no significant influence on the uncertainty of the molar mass and of the respective isotope ratios and measured intensity ratios. This is a consequence of the dominating mass bias of the isotope ratio  $R_x(^{30}\text{Si}/^{29}\text{Si})$  in the sample which is two orders of magnitude different from unity in case of this crystal. The application and impact of tau correction in case of using  $10^{13}$   $\Omega$  amplifiers can be neglected when operating with stable input signals from continuous ion beams in contrast to transient signals (e.g. as known from laser ablation). When diluting the original sample solutions (here: from  $w = 4536$   $\mu\text{g g}^{-1}$  down to  $1134$   $\mu\text{g g}^{-1}$ ), the use of  $10^{13}$   $\Omega$  amplifiers opens the door for the measurement of isotope ratios of enriched silicon in this concentration range maintaining the uncertainty associated with  $M$ . This study shows that a dilution of the extremely high mass fractions used in the measurements of the molar mass of enriched silicon is possible when applying the high ohmic  $10^{13}$   $\Omega$  amplifier setups. This will strongly improve the experiment (reduction of clogging, increase of beam stability), enabling longer duration of measurements (sequences) and less stress toward the mass spectrometer. The main benefit of the use of  $10^{13}$   $\Omega$  amplifiers is the possibility of using smaller (factor  $\approx 0.25$ ) sample sizes, enabling less sample preparation time and material costs while keeping the level of uncertainty and improving the possibility of detecting local isotopic variations. Also, in the near future silicon crystals even more depleted in  $^{30}\text{Si}$  will be analysed using the  $10^{13}$   $\Omega$  amplifier setup.

## Conflicts of interest

There are no conflicts of interest to declare.

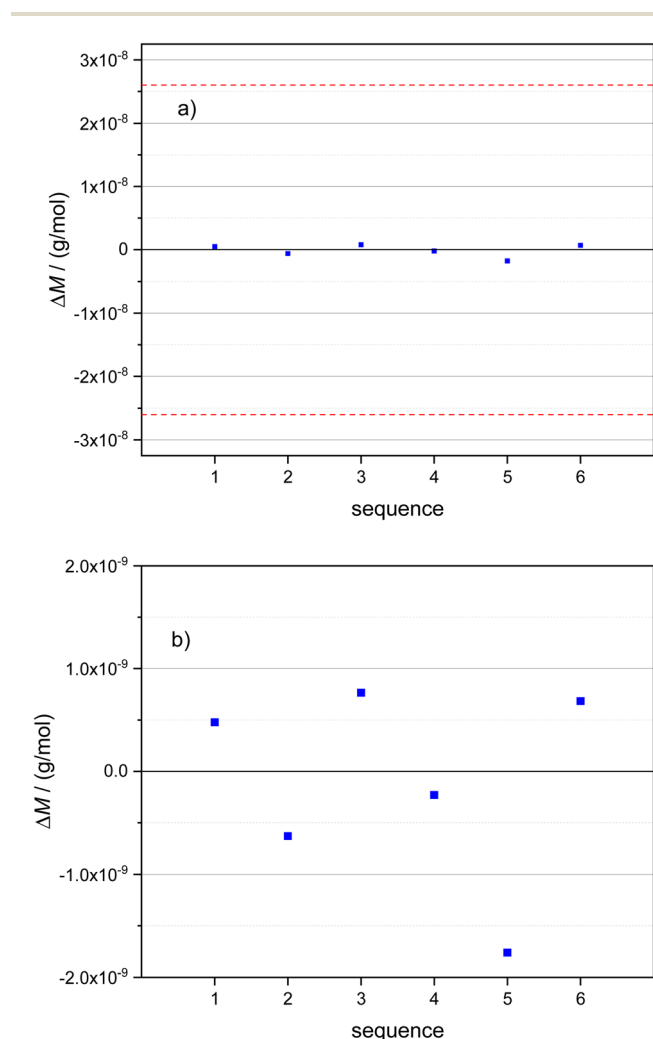


Fig. 9 Influence of  $\tau$  correction applied to isotope ratios for molar mass results (sample N.2.1). (a) Shows the absolute difference  $\Delta M = M_{n\tau} - M_\tau$ : blue squares of the six sequences. The red dashed area depicts the area of the average uncertainty associated with  $M_\tau$ . (b) Is a zoom of (a) and shows more clearly the range of the difference between tau corrected and non-corrected  $M$  values of the sample N.2.1. This range is one order of magnitude smaller than the uncertainty range given in (a) proving that a possible signal delay on different Faraday detectors equipped with  $10^{13}$   $\Omega$  resistors does not influence/bias the isotope ratios and molar masses of this study significantly.



## Acknowledgements

The authors gratefully acknowledge the provision of silicon crystal samples by Daniela Eppers (PTB). Many thanks also to Grant Craig (Thermo Fisher Scientific Bremen GmbH) for helpful advice concerning the tau correction.

## References

- 1 J. M. Koornneef, C. Bouman, J. B. Schwieters and G. R. Davies, Measurement of small ion beams by thermal ionisation mass spectrometry using new  $10^{13}$   $\Omega$  resistors, *Anal. Chim. Acta*, 2014, **819**, 49–55.
- 2 A. Trinquier, *Gain Calibration Protocol for  $10^{13}$   $\Omega$  Resistor Current Amplifiers Using the Certified Neodymium Standard JNd-1 on the TRITON Plus*, Application Note 30285, Thermo Fisher Scientific Inc., 2014.
- 3 C. Bouman, A. Trinquier, N. Lloyd, J. Schwieters, J. Koornneef and G. Davies, *New Design  $10^{13}$   $\Omega$  Amplifiers for Measurement of Small Ion Beam Currents*, Application Note 30282, Thermo Fisher Scientific Inc., 2015.
- 4 T. Breton, N. S. Lloyd, A. Trinquier, C. Bouman and J. B. Schwieters, Improving precision and signal/noise ratios for MC-ICP-MS, *Procedia Earth Planet. Sci.*, 2015, **13**, 240–243.
- 5 M. Klaver, R. J. Smeets, J. M. Koornneef, G. R. Davies and P. Z. Vroon, Pb isotope analysis of ng size samples by TIMS equipped with a  $10^{13}$   $\Omega$  resistor using a  $^{207}\text{Pb}$ – $^{204}\text{Pb}$  double spike, *J. Anal. At. Spectrom.*, 2016, **31**, 171–178.
- 6 E. Plomp, I. C. C. von Holstein, J. M. Koornneef, R. J. Smeets, L. Font, J. A. Baart, T. Forouzanfar and G. R. Davies, TIMS analysis of neodymium isotopes in human tooth enamel using  $10^{13}$   $\Omega$  amplifiers, *J. Anal. At. Spectrom.*, 2017, **32**, 2391–2400.
- 7 H. Vollstaedt, G. Craig, N. Lloyd, J. Schwieters and C. Bouman,  *$10^{13}$   $\Omega$  Amplifier Technology: How Low Can You Go? Smart Note SN30439*, Thermo Fisher Scientific Inc., 2017.
- 8 G. Wang, H. Vollstaedt, J. Xu and W. Liu, High-Precision Measurement of  $^{187}\text{Os}/^{188}\text{Os}$  Isotope Ratios of Nanogram to Picogram Amounts of Os in Geological Samples by N-TIMS using Faraday Cups Equipped with  $10^{13}$   $\Omega$  Amplifiers, *Geostand. Geoanal. Res.*, 2019, **43**, 419–433.
- 9 M. Dellinger, R. G. Hilton and G. M. Nowell, Measurements of rhenium isotopic composition in low-abundance samples, *J. Anal. At. Spectrom.*, 2020, **35**, 377–387.
- 10 J. B. Creech, B. F. Schaefer and S. P. Turner, Application of  $10^{13}$   $\Omega$  Amplifiers in Low-Signal Plasma-Source Isotope Ratio Measurements by MC-ICP-MS: A Case Study with Pt Isotopes, *Geostand. Geoanal. Res.*, 2020, **44**, 223–229.
- 11 K. Yamamoto, H. Asanuma, H. Takahashi and T. Hirata, *In situ* isotopic analysis of uranium using a new data acquisition protocol for  $10^{13}$  ohm Faraday amplifiers, *J. Anal. At. Spectrom.*, 2021, **36**, 668–675.
- 12 J.-I. Kimura, Q. Chang, N. Kanazawa, S. Sasaki and B. S. Vaglarov, High-precision in situ analysis of Pb isotopes in glasses using  $10^{13}$   $\Omega$  resistor high gain amplifiers with ultraviolet femtosecond laser ablation multiple Faraday collector inductively coupled plasma mass spectrometry, *J. Anal. At. Spectrom.*, 2016, **31**, 790–800.
- 13 M. Pfeifer, N. S. Lloyd, S. T. M. Peters, F. Wombacher, B.-M. Elfers, T. Schulze and C. Münker, Tantalum isotope ratio measurements and isotope abundances determined by MC-ICP-MS using amplifiers equipped with  $10^{10}$ ,  $10^{12}$ , and  $10^{13}$   $\Omega$  resistors, *J. Anal. At. Spectrom.*, 2017, **32**, 130–143.
- 14 R. Grigoryan, M. Costas-Rodríguez, P. Santens and F. Vanhaecke, Multicollector Inductively Coupled Plasma–Mass Spectrometry with  $10^{13}$   $\Omega$  Faraday Cup Amplifiers for Ultrasensitive Mg Isotopic Analysis of Cerebrospinal Fluid Microsamples, *Anal. Chem.*, 2020, **92**, 15975–15981.
- 15 O. Rienitz and A. Pramann, Comparison of the isotopic composition of silicon crystals highly enriched in  $^{28}\text{Si}$ , *Crystals*, 2020, **10**, 500.
- 16 K. Fujii, H. Bettin, P. Becker, E. Massa, O. Rienitz, A. Pramann, A. Nicolaus, N. Kuramoto, I. Busch and M. Borys, Realization of the kilogram by the XRCD method, *Metrologia*, 2016, **53**, A19–A45.
- 17 G. Bartl, et al., A new  $^{28}\text{Si}$  single crystal: counting the atoms for the new kilogram definition, *Metrologia*, 2017, **54**, 693–715.
- 18 B. Güttler, O. Rienitz and A. Pramann, The Avogadro constant for the definition and realization of the mole, *Ann. Phys.*, 2018, 1800292.
- 19 O. Rienitz, A. Pramann and D. Schiel, Novel concept for the mass spectrometric determination of absolute isotopic abundances with improved measurement uncertainty: Part 1 – theoretical derivation and feasibility study, *Int. J. Mass Spectrom.*, 2010, **289**, 47–53.
- 20 G. Mana and O. Rienitz, The calibration of Si isotope-ratio measurements, *Int. J. Mass Spectrom.*, 2010, **291**, 55–60.
- 21 A. Pramann, K.-S. Lee, J. Noordmann and O. Rienitz, Probing the homogeneity of the isotopic composition and molar mass of the “Avogadro”-crystal, *Metrologia*, 2015, **52**, 800–810.
- 22 L. Yang, Z. Mester, R. E. Sturgeon and J. Meija, Determination of the Atomic Weight of  $^{28}\text{Si}$ -Enriched Silicon for a Revised Estimate of the Avogadro Constant, *Anal. Chem.*, 2012, **84**, 2321–2327.
- 23 T. Narukawa, A. Hioki, N. Kuramoto and K. Fujii, Molar-mass Measurement of a  $^{28}\text{Si}$ -enriched silicon crystal for determination of the Avogadro constant, *Metrologia*, 2014, **51**, 161–168.
- 24 R. D. Vocke Jr, S. A. Rabb and G. C. Turk, Absolute silicon molar mass measurements, the Avogadro constant and the redefinition of the kilogram, *Metrologia*, 2014, **51**, 361–375.
- 25 T. Ren, J. Wang, T. Zhou, H. Lu and Y.-j. Zhou, Measurement of the molar mass of the  $^{28}\text{Si}$ -enriched silicon crystal (AVO28) with HR-ICP-MS, *J. Anal. At. Spectrom.*, 2015, **30**, 2449–2458.
- 26 BIPM, IEC, IFCC, ILAC, ISO, IUPAC, IUPAP and OIML, Evaluation of measurement data – Guide to the expression of uncertainty in measurement, *JCGM 100:2008*, 2008.



- 27 M. Wang, W. J. Huang, F. G. Kondev, G. Audi and S. Naimi, The AME2020 atomic mass evaluation, *Chin. Phys. C*, 2021, **45**, 030003.
- 28 A. Pramann, J. Noordmann and O. Rienitz, Investigation of mass-scale drift effects in the milli-mass range: Influence on high mass resolution mode multicollector-inductively coupled plasma mass spectrometer isotope ratio measurements, *J. Mass Spectrom.*, 2021, **56**, e4732.
- 29 G. Craig, Z. Hu, A. Zhang, N. S. Lloyd, C. Bouwman and J. Schwieters, *Dynamic Time Correction for High Precision Isotope Ratio Measurements*, Technical Note 30396, Thermo Fisher Scientific Inc., 2019.
- 30 T. Pettke, F. Oberli, A. Audétat, U. Wiechert, C. R. Harris and C. A. Heinrich, Quantification of transient signals in multiple collector inductively coupled plasma mass spectrometry: accurate lead isotope ratio determination by laser ablation of individual fluid inclusions, *J. Anal. At. Spectrom.*, 2011, **26**, 475–492.
- 31 A. Gourgiotis, G. Manhès, P. Louvat, J. Moureau and J. Gaillardet, Transient signal isotope analysis using multicollection of ion beams with Faraday cups equipped with  $10^{12} \Omega$  and  $10^{11} \Omega$  feedback resistors, *J. Anal. At. Spectrom.*, 2015, **30**, 1582–1589.
- 32 A. Gourgiotis, G. Manhès, P. Louvat, J. Moureau and J. Gaillardet, Transient signal isotope analysis: validation of the method for isotope signal synchronization with the determination of amplifier first-order time constants, *Rapid Commun. Mass Spectrom.*, 2015, **29**, 1617–1622.

